RFID Antennas for the UHF Remote Monitoring of Human Subjects

Gaetano Marrocco, *Member, IEEE*

***Abstract*—This paper addresses the design of passive and semi-passive transponder antennas for radio frequency identification applications involving the human body as the object to be tagged or bio-monitored. A planar tag antenna geometry, that is based on a suspended patch fed via a nested slot and is able to host sensors and electronics, is here introduced. Guidelines for conjugate impedance matching are given for different kinds of microchip transmitters, within power limitations as well as space constraints. Finally, the antenna matching performance is experimentally evaluated utilizing a body-tissue phantom.**

***Index Terms*—Impedance matching, planar antenna, radio frequency identification (RFID), sensor networks, slot antenna.**

I. Introduction

RADIO frequency identification (RFID) of objects and remote control of devices has become very popular in logistics, inventory management and bioengineering applications. Various kinds of data can be wireless transferred to a local querying system (reader) from a remote transponder (tag) that includes an antenna and a microchip transmitter. A new frontier in this area is the wireless monitoring of people within mobile healthcare services [1]–[5]. Thanks to the advances in low-power electronics, it is now feasible to envisage sophisticated RFID-like devices integrating sensing and signal processing ability [6]–[8], in addition to more traditional tagging operations. Such RFID systems could provide real-time bio-monitoring (temperature, blood pressure, heartbeat, glucose content, human behavior) and tracking of a person's movement within hospitals or domestic environments, as well as inside extreme places such as a Space Capsule. These devices could be *passive*, harvesting energy from the interrogating system, *semi-active* when a battery is included only to feed the sensors, or fully *active* [9] where a local source directly feeds a microcontroller as well as the transmitting radio. However, the large battery packs required for active techniques, in addition to the use of protruding antennas, are suboptimal for medical use and additional issues have to be considered, such as the compromise between a long battery-life and a miniaturized design [8]. Moreover, when active tags are attached onto the human body, or implanted, the resultant RF power deposition inside tissue must be compliant with safety regulations [10].

Focusing on passive or semi-active systems, many RFID tag antennas, for on-body application or implants, conventionally work in the HF band (13.56 MHz) or below. These devices are typically fabricated as multi-turn coils, [11] as in the case of wristbands or insulated capsules. At this frequency the antenna performs well around liquids and human tissues but the activation range is generally smaller than 1 m due to the fast attenuation of the magnetic field with the distance. On the other hand, UHF devices (860–960 MHz), although more influenced by high dielectric targets, may in principle promise larger activation ranges.

Together with the microchip sensitivity, the tag antenna plays a key role in the RFID system performance, such as the reading range and compatibility with the tagged object. In the case of RFID with sensing capability, the antenna should be additionally suited for electrical and physical integration with sensor electronics.

Antennas for UHF omnidirectional tags are typically designed as modified printed dipoles. To miniaturize the size and achieve inductive input reactance required for microchip impedance matching, modified meander line configurations are commonly adopted [12]–[14]. Meander line antennas are however not well suited to host sensors. PIFA and IFA like antennas [15]–[17], requiring a ground plane, could instead provide space to allocate electronics and they have been already experimented as conventional tags attached over dielectric and metallic objects. Nevertheless, since they work as miniaturized antennas, small bandwidth and poor efficiency are expected. Miniaturization is however not the most critical issue in *on-body* application in the UHF band.

Conventional general-purpose tags are designed in free space, but when on-body applications are required, the strong pattern distortion and the efficiency loss, caused by human body dissipation and scattering, need to be taken into account in the first stage of the design. Although considerable publications are available about on-body antennas used for microwave heating [18] as well as for radiometric [19] and radar sensors [20] and for implanted devices [10], [21], the design of UHF RFID antennas for on-body applications is not a common topic since it involves conjugate impedance matching to microchip transmitters having high capacitive input reactance.

This contribution addresses the design of planar antennas placed onto the human body working in the UHF RFID band and introduces a tag antenna configuration of simple geometry having impedance tuning capability and the possibility to host electronics packaging. In Section II, energetic and technological constraints, which must be considered in order to allow activation of a passive on-body tag with a given antenna gain, are discussed. The proposed antenna geometry, a suspended patch sourced via a nested shaped slot, is evaluated with reference to simplified human models in Section III. Guidelines and design

Manuscript received October 3, 2006; revised March 12, 2007.

The author is with the Dipartimento di Informatica, Sistemi e Produzione, Università di Roma Tor Vergata, Via del Politecnico, 1, 00133 Roma (e-mail marrocco@disp,uniroma2.it).

Digital Object Identifier 10.1109/TAP.2007.898626

charts are then given for matching the antenna to complex loads (Section IV). Next, some examples permit discussion of the matching properties in the case of a low- and high-impedance microchip, the performance sensitivity to human body size (Section V), and the maximization of the available space for sensor packaging (Section VI). Finally, an experimental study on fabricated prototypes (Section VII) validates the numerical investigation.

II. Energetic Constraints

Having fixed the effective power $(EIRP_R)$ transmitted by the reader and the sensitivity $(P_{\rm chip})$ of the tag microchip (i.e. the RF power required to the microchip electronics to turn on and to perform back-scattering modulation), the maximum activation distance of the tag along the (θ, ϕ) direction [22] is given by

$$d_{\max}(\theta,\phi) = \frac{c}{4\pi f}\sqrt{\frac{EIRP_R}{P_{\rm chip}}\tau G_{\rm tag}(\theta,\phi)} \tag{1}$$

where $G_{\rm tag}(\theta,\phi)$ is the tag gain and the factor

$$\tau = \frac{4R_{\rm chip}R_A}{|Z_{\rm chip}+Z_A|^2} \le 1 \tag{2}$$

is the power transmission coefficient which accounts for the impedance mismatch between the antenna $(Z_A = R_A + jZ_A)$ and microchip $(Z_{\rm chip} = R_{\rm chip} + jZ_{\rm chip})$. Since the microchip includes an energy storage stage, its input reactance is strongly capacitive. Most of the available RFID microchips in the UHF band exhibit an input reactance roughly ranging from $-100\ \Omega$ to $-400\ \Omega$ or more, while the real part is about an order of magnitude smaller or less. Thus, the antenna impedance should be inductive in order to achieve conjugate matching. Beyond the distance $d_{\max}$ the power collected by the tag falls below the microchip sensitivity and the tag is unreachable.

The presence of the human body with its high permittivity and conductivity will be advantageous for antenna miniaturization but will also induce strong power absorption with respect to free space.

The maximum radiated power by the reader is constrained to local regulations, in particular 3.2 W EIRP within the 865.6-867.6 MHz band (Europe) and 4 W EIRP within 902–928 MHz (USA).

Microchip sensitivity is continuously improving, reducing from 1 mW in the year 2001 to some tenths of a microwatt in today's current products, or even less in the state of the art ASICS [23].

From (1) it can be deducted that, according to the European regulations, antennas with $\tau G_{\rm tag} \le -10$ dB could achieve a maximum reading distance of 5 m or more, which is in principle suited to human body monitoring within a medium-size room, provided that the microchip sensitivity is less than 10 μW. Even longer links can be obtained according to the US regulations.

III. The Nested-Slot Suspended Patch

The proposed antenna layout is an H-shaped slot placed onto a suspended patch, hereafter denoted as nested-slot suspended patch (NSSP) antenna (Fig. 1). This layout is able to host sensors and, thanks to the small slot, inductive reactance can be easily achieved. To electrically isolate the antenna from the skin, and to permit tag bio-compatibility, it is assumed that the tag will be attached onto the body through a thin silicone substrate. Since the slot sizes are comparable with the patch surface, the radiation features are related to both the slot and patch size. In particular, the maximum antenna gain is mainly fixed by the patch side L, while the impedance tuning can be changed by acting on the slot sizes a and b.

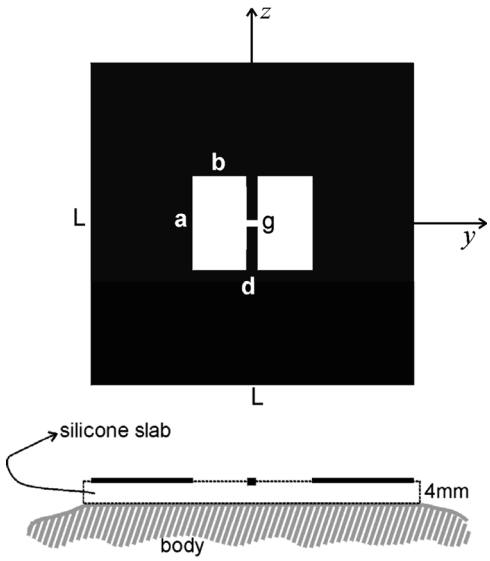

Fig. 1. Geometry of the proposed nested-slot suspended-patch antenna. The microchip transmitter should be placed in the central gap having size $g \times d$.

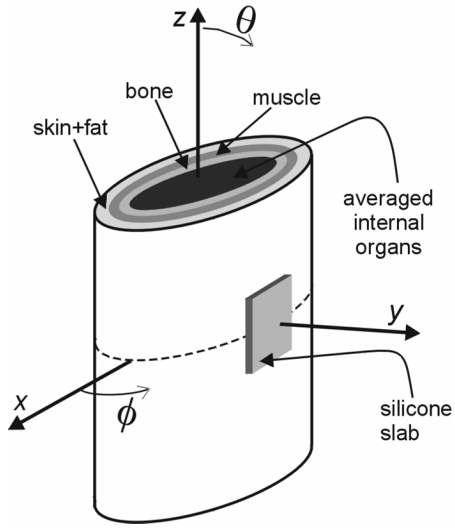

Fig. 2. Stratified elliptical cylinder model of the human thorax for the design of bio-compatible tags. The size of the cylindrical cross-sections is reported in Table I. Cylinder height: 40 cm.

Just for example, it is hereafter supposed that the tag is attached onto the human torso. However, the same design methodology can be extended to different body regions. For the purpose of antenna design, a simplified reference model of the human torso defined as a stratified elliptical cylinder (Fig. 2) with physical parameters (Table I) obtained from tissue database in [24], is considered. Two different torso sizes are used, referred to as *thin*

Table I
PHYSICAL AND GEOMETRICAL PARAMETERS OF THE LAYERED ANATOMICAL MODEL IN FIG. 2 AT 870 MHz

Layer	ε_r	σ [S/m]	Ellipse axis *thin man* [cm]	Ellipse axis *thick man* [cm]
Skin+fat	14.5	0.25	33.5×16.8	50.0×20.0
Muscle	55.1	0.93	31.0×14.2	46.5×17.0
Bone	20.8	0.33	28.4×10.5	42.6×12.6
Internal organs	52.1	0.91	27.2×8.4	41.0×10.0

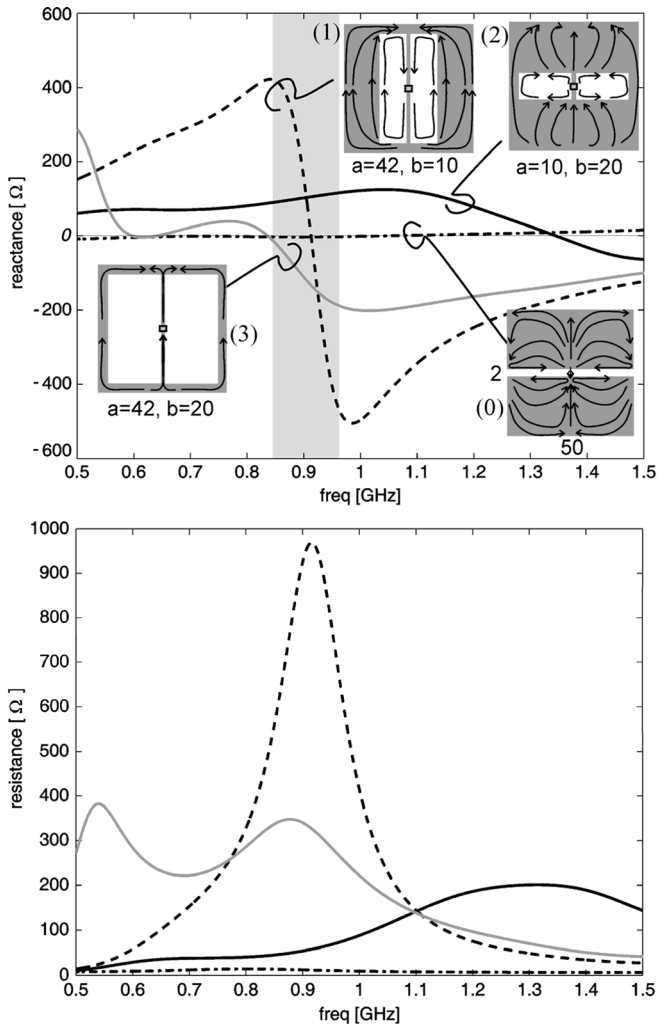

Fig. 3. Antenna input impedance for some choice of the H-slot parameters (size in [mm]). In all the cases the fixed sizes are $L = 50$ mm, $d = g = 2$ mm, and the *thin-man* model is considered. Arrows indicate the flow of the surface current density at 870 MHz. The shadowed strip defines the RFID band covering all regions of the world.

man, resembling a boy or a woman, and as *thick man*. These configurations have been preferred to a more conventional layered or homogeneous half-space geometry with the intent of evaluating the tag gain, and hence the activation range, also in the back and on the side of the body.

Depending on the shape and on the size of the internal slot, the antenna mainly acts either as a square dipole, a *dumbbell* H-slot [25], a broadband patch or as a doubly folded dipole. The impedances in Fig. 3 are shown for antennas of external size $L = 50$ mm placed onto the body through a 4 mm-thick silicone slab with parameters $\varepsilon = 11.9$ and $\sigma = 0.0$. All of the electromagnetic analyses are performed by means of the FDTD method [26], having modeled the *thin-man* in the free space. The patch is considered to be copper, with ohmic losses taken into account in the numerical simulations by means of the superficial impedance.

A. Square Dipole Mode

The limiting case of a square planar dipole is obtained (Fig. 3, case 0) when the slot degenerates into a gap ($a = g \ll \lambda$ and $2b + d = L$). Such an antenna, which is nearly resonant in the RFID UHF band, presents a small reactance to achieve impedance matching to the microchip. The antenna gain has been found to be rather distorted with respect to the free space, ranging from -6.3 dB in front of the antenna ($\phi = 90°$), to -13 dB along the side ($\phi = 0°$) and to -17.6 dB along the cylinder rear ($\phi = -90°$). For this antenna, the body model and silicone slab act as an $\varepsilon_e = 6.5$ effective permittivity medium (the same antenna resonates at 1.8 GHz in the free space, instead of 0.7 GHz when attached to the torso model).

B. Dumbbell Mode ($b \ll L$)

When the slot width b is sensibly smaller than the external side L (Fig. 3, case 1), a typical RLC behavior can be observed with strong reactance peaks. The resonant frequency can be roughly related to the H-slot sizes, [27], [28], through $f_0 = c/(2\pi)\sqrt{g/(abd\varepsilon_e)}$. As the size b increases, the resonance moves toward the DC and the reactance's peak reduces. The input resistance is quite large close to the resonant frequency. The vertical surface electric current density (at 870 MHz) on the patch is not equi-verse and therefore the antenna maximum gain is reduced ($G_{\max} = -7.4$ dB) with respect to the square dipole.

C. Broadband Patch Mode ($2b \approx L$)

When the slot width is nearly similar to the antenna side (Fig. 3, case 2), the flow of the vertical component of the surface current is unchanged on the whole conductor, as in a patch geometry, and the antenna gain ($G_{\max} = -7.0$ dB) is slightly larger than in the previous configuration. The input reactance exhibits values of the order of 100 Ω, still larger than in the case of the square dipole. This reactance is slowly variable with the frequency and in particular it remains nearly constant within the 860–960 MHz band (which includes Europe, USA and the RFID frequency allocation of other countries).

D. Doubly-Folded Dipole Mode ($2b \approx a \approx L$)

When the size a and b increase until the slot fills nearly the whole patch surface (Fig. 3, case 3), a folded dipole mode ($G_{\max} = -6.6$ dB) is achieved but the reactance becomes capacitive in the band of interest, and therefore it is not suited to achieve conjugate matching to the microchip transmitter.

An increase in the size d of the sourced conductor mainly provides a capacitive contribution to the tag impedance, and it will be fixed to a thin value ($d = 2$ mm) in all the examples considered.

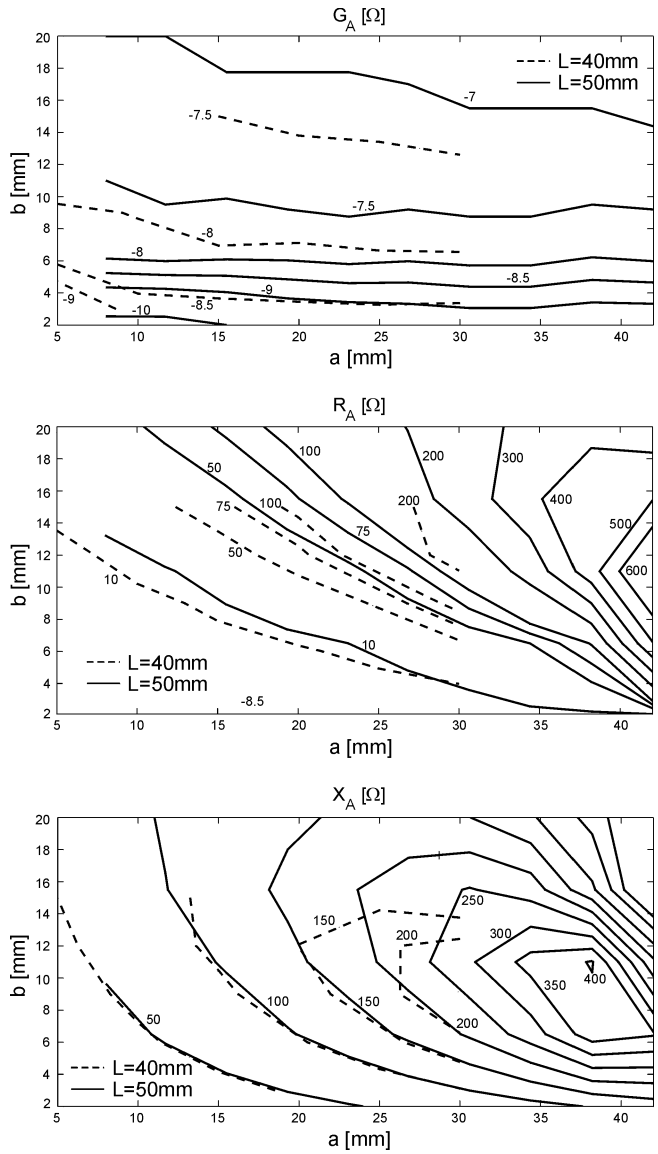

Fig. 4. Parametric exploration of maximum gain (at $\phi = 90°$, $\theta = 90°$) and input impedance of the NSSP antenna when changing the slot size $\{a, b\}$ and keeping the other parameters fixed to $L = \{40\ \mathrm{mm}, 50\ \mathrm{mm}\}$, $d = 2\ \mathrm{mm}$ and $g = 2\ \mathrm{mm}$. Frequency: 870 MHz. Thin-man model.

IV. Conjugate Matching Performance

The NSSP antenna features are explored here by relating the input impedance and gain to the geometrical parameters with the goal of obtaining impedance charts for conjugate matching to typical RFID microchips.

Fig. 4 shows the variation in impedance and maximum gain when the H-slot aspect ratio $\{a, b\}$ is changed, for the cases of $L = 40\ \mathrm{mm}$ and $L = 50\ \mathrm{mm}$ antennas used with the thin-man model. It can be observed that the gain variation is mainly related to the size b, while the reactance and the inductance are affected by both a and b, showing a broad and non-monotonic behavior. A similar result has also been found for different external sizes of the antenna $L = \{30\ \mathrm{mm}, 60\ \mathrm{mm}\}$, where the impedance variation is reduced (small L) or enlarged (large L).

Table II
Power Transmission Coefficients of the NSSP Antenna, When Fed to Different Microchip Transmitters

Chip	Z_{chip} [Ω]	τ L=40	τ L=50	τ L=60
[29]	73-j113	1.00	1.00	1.00
[30]	6-j127	0.93	0.93	0.95
[23]	40-j366	0.50	0.85	0.86
[15]	7-j170	0.68	0.80	0.82
EM 4223	19-j285	0.57	0.78	0.80
Phillips Ucode G2	20-j300	0.45	0.75	0.78
[31]	6-j220	0.35	0.54	0-74
Phillips EPC 1.13	16-j350	0.28	0.54	0.74
Phillips SL3530	12-j457	0.10	0.26	0.54

A proper choice of these parameters therefore offers some degree of freedom to achieve conjugate matching to the microchip transmitter. This is demonstrated in Table II where the slot sizes have been chosen from Fig. 4 to maximise the power transmission coefficient τ to some typical microchips. The *thin-man* torso model is still considered in this case.

It can be observed that the $L = 50{-}60\ \mathrm{mm}$ antennas permit a larger matching freedom than the $L = 40\ \mathrm{mm}$ configuration, and a τ factor larger than 0.75 has been obtained in most of the cases. Matching performance deteriorates ($\tau < 0.5$), even with $L = 60\ \mathrm{mm}$ designs, for those microchips having both a large impedance phase angle and large reactance. It is however expected that better performance could also be obtained by adding further degrees of freedom to the slot shape, for instance by introducing properly optimized multiple ridges instead of the single central one.

In general it is shown that matching capabilities improve for large L configurations.

To further investigate the features of the NSSP antennas with respect to the external size L, two layouts obtained from the matching charts in Fig. 4 are now considered in full detail. The first configuration is matched to a microchip (referred to as chip.1) with small impedance phase angle $Z_{\mathrm{chip},1} = 73 - j113\ \Omega$ [29], while the second configuration utilizes a microchip (chip.2) with a high impedance phase angle $Z_{\mathrm{chip},2} = 40 - j336\ \Omega$ [23].

The best matched antennas to chip.1 show a mainly horizontal H-slot (Fig. 5) with a power transmission coefficient τ almost unitary, provided that the external side L is larger than 30 mm. The vertical size of the slot mainly affects the reactance and remains nearly unchanged when increasing the patch side. Assuming a chip sensitivity of 100 μW, the maximum reading distance is about $d_{\max} = 2.0\ \mathrm{m}$ for the $L = 50\ \mathrm{mm}$ patch. The maximum distance becomes larger than $d_{\max} = 5.0\ \mathrm{m}$, even for the smallest $L = 30\ \mathrm{mm}$ tag, in the case of microchips with a sensitivity of 10 μW or less.

When using the high impedance phase angle chip (Fig. 6) the matching H-slot has a predominantly vertical size while the width b decreases as the external length L enlarges in order to keep the antenna input resistance low. The maximum activation distance which can be obtained with this high performance chip

Chip 1 Z_{chip}= 73-j113Ω	L=30mm	L=40mm	L=50mm
			
	a=16.2mm b=10mm	a=15mm b=15mm	a=15.1mm b=20mm
Z_A [Ω]	31+j129	76+j133	78+j120
τ	0.8	0.99	0.99
G_{max} [dB]	-8.5	-7.5	-6.9
d_{max} [m]:			
P_{chip}=100μW	1.7	2.0	2.1
P_{chip}=10μW	5.3	6.3	6.7

Fig. 5. Best-matched antennas to a chip having small input impedance phase angle $(-57°)$. Frequency f = 870 MHz. EIRP = 3.2 W. *Thin-man* torso model.

Chip 2 Z_{chip}= 40-j366Ω P_{chip}=2.7μW	L=30mm	L=40mm	L=50mm
			
	a=20mm b=10mm	a=30mm b=9mm	a=38.2mm b=6.5mm
Z_A [Ω]	57+j177	114+j253	86+j346
τ	0.20	0.50	0.84
G_{max} [dB]	-8.4	-7.7	-7.8
d_{max} [m]	5.1	8.7	10.8

Fig. 6. Best-matched antennas to a chip having large input impedance phase angle $(-83°)$. Frequency f = 870 MHz, EIRP = 3.2 W. *Thin-man* torso model.

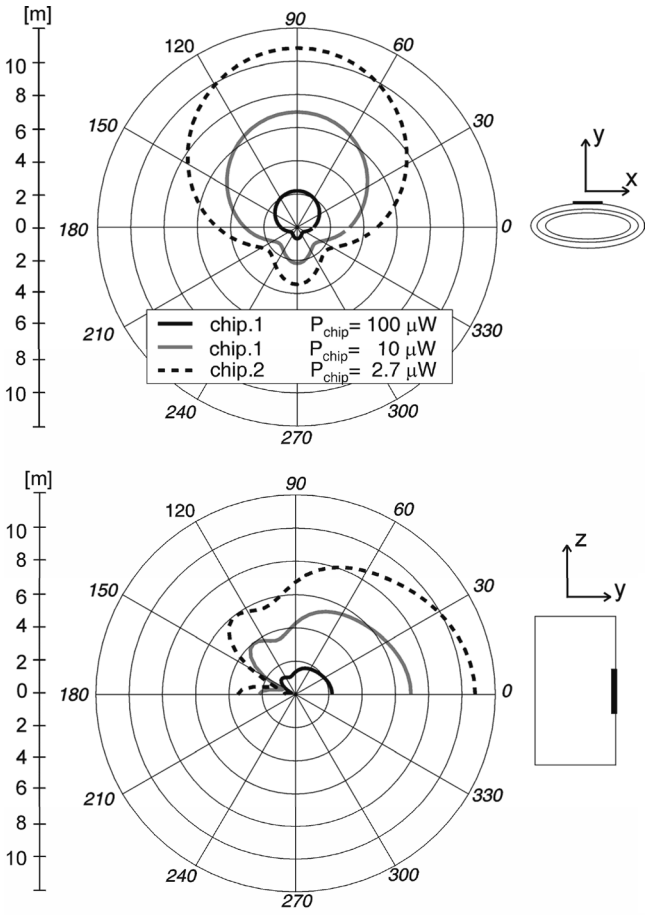

Fig. 7. Activation regions $r(\theta,\phi) < d_{\max}(\theta,\phi)$ on the horizontal and vertical planes for the $L = 50$ mm antennas in Fig. 5 and Fig. 6 as computed from (1), having supposed $\mathrm{EIRP_R} = 3.2$ W and the *thin-man* model.

($P_{\text{chip}} = 2.7$ μW, [23]) is theoretically more than 8 m ($L \geq 40$ mm).

The activation region $r(\theta,\phi) < d_{\max}(\theta,\phi)$, i.e. the volume where the power collected by the tag is larger than the chip sensitivity, is shown in Fig. 7 for the $L = 50$ mm antennas and having assumed a 3.2 W EIRP radiated by the reader. It can be observed that, with low-power microchips ($\mathrm{P_{chip}} < 10$ μW), the useful activation regions are quite significant all around the body.

V. Antenna Sensitivity to Target Size

An important issue is the change in the impedance matching of the NSSP antenna when a different sized body is to be tagged. In the following numerical experiment, two $L = 50$ mm antennas (one involving chip.1 and the other chip.2) have been optimized for maximum τ at 870 MHz utilizing the thin-man model. Afterward, the same antennas have been evaluated on the thick-man torso. The matching performance for these cases is shown in Fig. 8. As expected from the impedance curves in Fig. 3, the power transmission coefficient associated with the horizontal H-slot coupled to chip.1 is only slightly frequency dependent. For this type of antenna the input impedance is quite unchanged over a broad band and thus is not significantly affected by the torso size. Instead, for the vertical H-slot configuration connected to chip.2, τ is rather sensitive to frequency changes, as well as to the torso size.

VI. Sensor Packaging

The previous sections considered NSSP antennas that are symmetric with respect to both the x and z axis. However this geometry offers additional degrees of freedom in the position of the slot and in the connection to the microchip. In particular, alternate configurations are possible which can increase the available space for additional electronics. Fig. 9 shows, for instance, a modified version of the geometry in Fig. 5 where the slot has been relocated close to one of antenna edges, leaving free more than half the metallization area. Also the position of the microchip has been moved to one of the slot sides in order to simplify the connection of the microchip transmitter to the sensor stage.

Having optimized the antenna shape to the thin-man model, the obtained power transmission factor is $0.85 < \tau < 0.95$ in the considered 860-960 MHz RFID band, while slightly smaller values $(0.80 < \tau < 0.85)$ are obtained when attaching the same

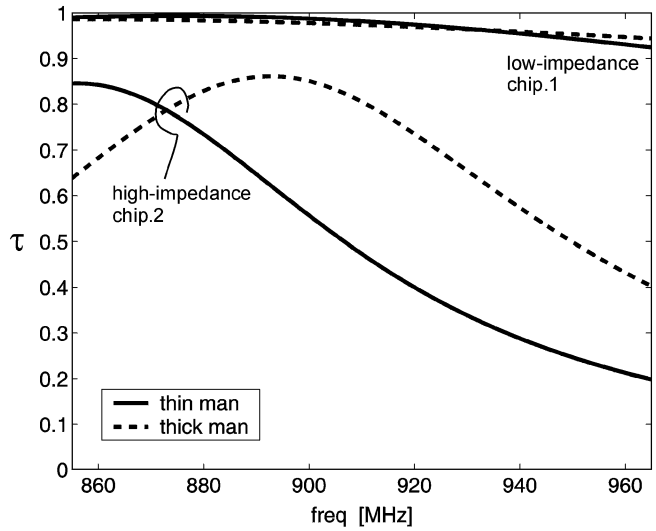

Fig. 8. Power transmission coefficient, in the world RFID band (including Europe, USA, and Japan) of the $L = 50$ mm antennas in Figs. 5 and 6 matched to their respective microchips at 870 MHz. Comparison between the thin- and thick-man cylindrical model.

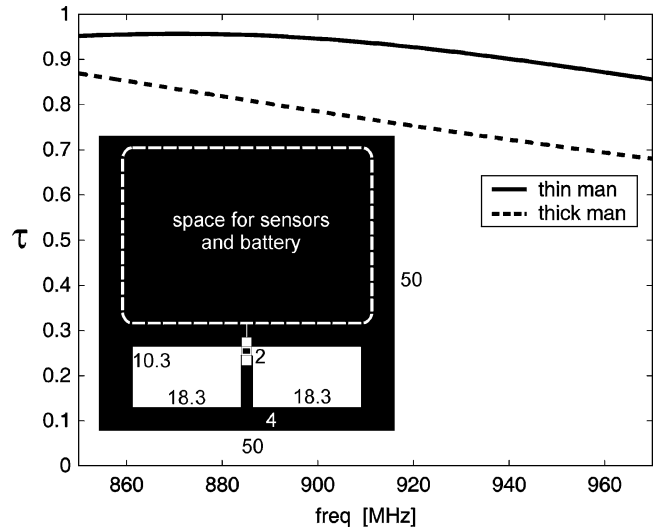

Fig. 9. Example of on-body tag (size in [mm]), matched to chip.1, having maximized the available space for sensors and battery.

antenna to the thick-man torso. The overall tag performances are nearly the same as for the centered slot configuration, but in the thick-man arrangement a lower antenna gain is achieved due to the stronger power absorption in a larger body. Similar results can be obtained when considering the tag that is matched to chip.2.

VII. Experimental Validation

The impedance matching features of the NSSP antenna have been experimentally verified on fabricated prototypes. To analyze the antenna independently of the microchip and reader characteristics, the input impedance of the antenna has been directly measured. In order to avoid the need of a balun, a monopole-like configuration has been considered with half the NSSP placed vertically over an image plane with a coaxial connector in the back face.

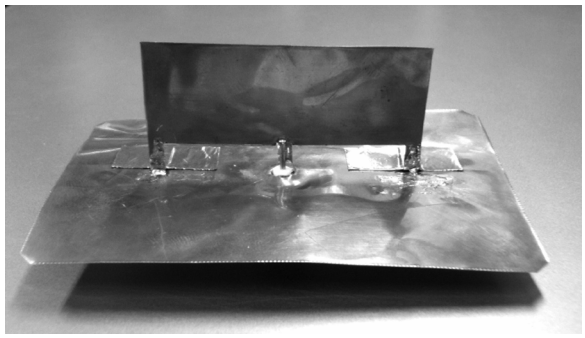

Fig. 10. Copper prototype of a NSSP antenna designed for a $20 \times 20 \times 20$ cm muscle-like box matched to chip.1. Antenna size, according to the geometry in Fig. 1: $L = 60$ mm, $a = 13$ mm, $b = 25$ mm, $g = 3$ mm, copper sheet thickness: 0.2 mm. Only a half-plane of the antenna has been fabricated since it is provided with an image plane. Coaxial (SMA) connector is in the reverse side of the image plane.

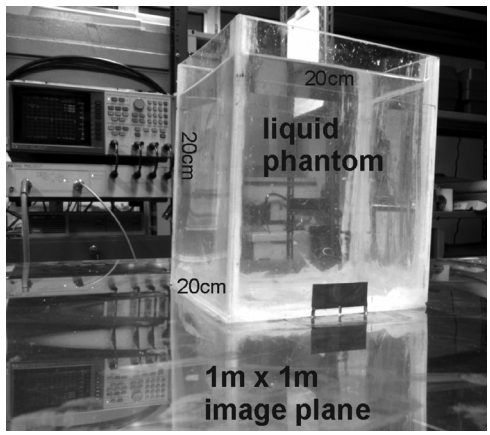

Fig. 11. Half-plane NSSP antenna in front of a Perspex cubic phantom filled with tissue-equivalent solution made of deionized water, saccharose and sodium chloride. The antenna and the box are placed over a 1 m × 1 m copper image plane.

The human body has been experimentally simulated by a simplified phantom used in previous studies on compliance tests of mobile communication devices [32], [33]. The phantom consists of a cubic box made of Perspex ($\varepsilon_{\rm r} = 2.1$, $\sigma = 0$) having 5 mm thickness and 20 cm width. The box is filled up to a height of 20 cm with a tissue-simulating liquid made with deionized water, saccharose and sodium chloride [34]. By different concentrations of these basic components, this phantom can represent the trunk of a child or even a human head.

The initial fabricated prototype is a $L = 60\,{\rm cm}$ NSSP antenna which has been specifically designed for a muscle-like phantom, (see the physical parameters in Table I) and has been optimized ($\tau = 0.97$ at 870 MHz) to the low-impedance phase angle chip ($Z_{{\rm chip},1} = 73 - j113\ \Omega$). The antenna has been fabricated by means of a 0.2 mm copper sheet (Fig. 10) directly attached onto the phantom‘s external side at the box-ground interface, as in Fig. 11. Due to the presence of the insulating Perspex layer, the silicon slab is not required to isolate the antenna from the liquid.

Measurements have been performed at the Toxicology and Biomedical Sciences Section of the ENEA Casaccia Research Centre. The dielectric parameters of the liquid phantom and the

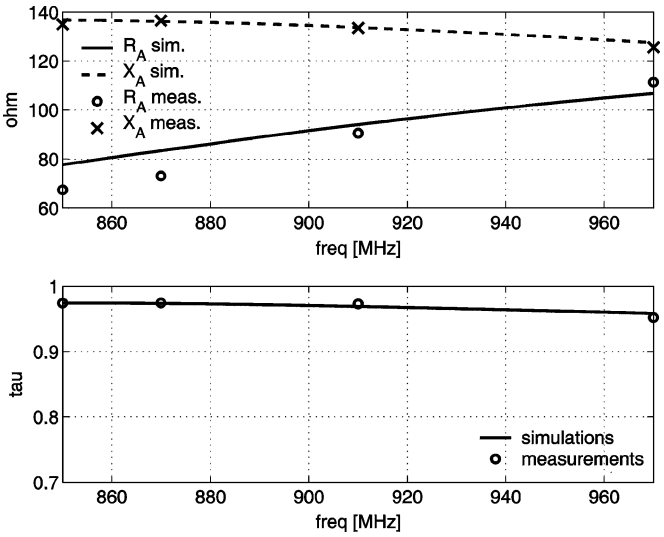

Fig. 12. Input impedance and power transmission coefficient for the 60 mm-side NSSP contacting the *muscle-like* liquid phantom ($\varepsilon_{\rm r} = 54.5 \pm 5\%$, $\sigma = 0.9 \pm 5\%$) when the antenna has been designed to be matched to chip.1 ($Z_{chip,1} = 73 - j113\ \Omega$). Data refer to the full-size antenna (measurement data have been doubled). Markers at 850, 870, 910, 950 MHz.

antenna impedance have been measured by means of an HP 85070 dielectric probe and an HP 8753C Vector Network Analyzer.

Fig. 12 shows the comparison, after the coaxial cable de-embedding, between the numerical simulations and the measured impedance for an experimental liquid phantom with muscle-like parameters ($\varepsilon_{\rm r} = 54.5 \pm 5\%$, $\sigma = 0.9 \pm 5\%$). Data refer to the full-size antenna, i.e. the measured impedance has been doubled.

Close agreement can be observed between the simulated model and the fabricated prototype in terms of the resistance and especially for the reactance. A better than 95% power transmission coefficient can be achieved in the world UHF RFID band.

Afterwards, to check the sensitivity of the antenna impedance when changing the body parameters, a second measurement was conducted for the same antenna coupled to a fluid with permittivity and conductivity $\varepsilon_{\rm r} = 44.9 \pm 5\%$ and $\sigma = 0.85 \pm 5\%$ (which could be representative of the human head). Resulting comparison of measurement and simulation (Fig. 13) shows that the matching condition is still preserved within the entire band considered.

A smaller, second prototype NSSP antenna was fabricated with size $\mathrm{L} = 50\ \mathrm{cm}$ and designed to be optimally matched to chip.1 when the antenna is attached to a head-like liquid phantom ($\varepsilon_{\rm r} = 44.9 \pm 5\%$ and $\sigma = 0.85 \pm 5\%$). The achieved power transfer coefficient τ is slightly worse than for the $L = 60\ \mathrm{mm}$ antenna. This is expected from the parametric analysis in Section IV where it is verified that the matching property of the NSSP antenna degrades with reduction in the antenna size. In this case good agreement with the simulated model (Fig. 14) is also observed, with the measured τ greater the 75% in the world RFID band

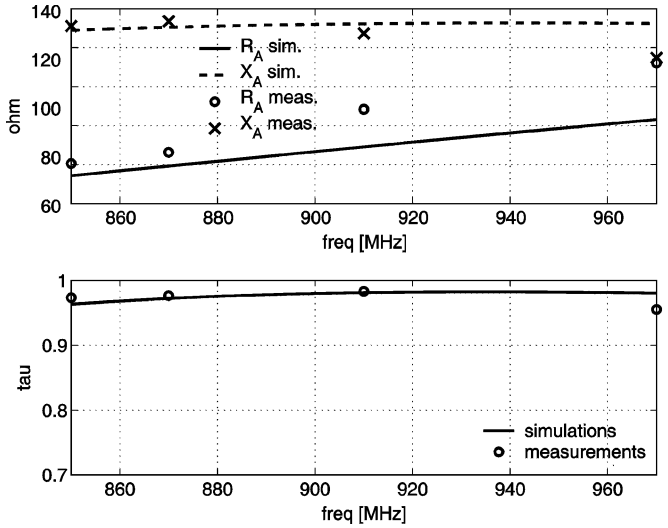

Fig. 13. Input impedance and power transmission coefficient for the 60 mm-side NSSP, which was designed for a muscle-like phantom, and is now measured and computed when the box is instead filled with a different fluid having parameters $\varepsilon_{\rm r} = 44.9 \pm 5\%$ and $\sigma = 0.85 \pm 5\%$. Markers are the same as in the previous diagrams.

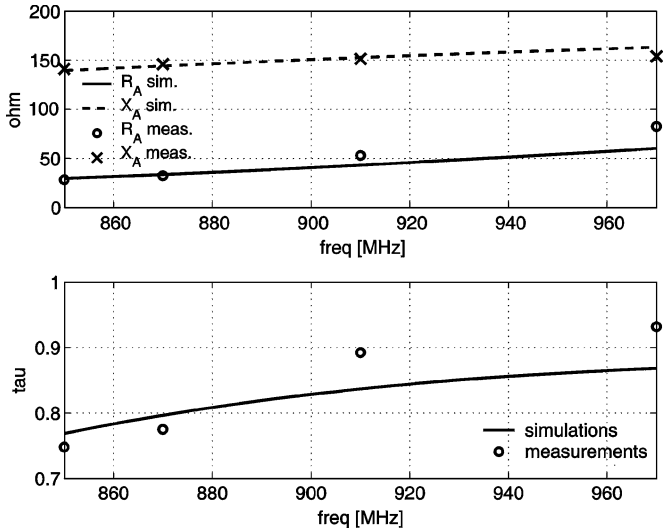

Fig. 14. Input impedance and power transmission coefficient for the 50 mm-side NSSP contacting the *head-like* liquid phantom ($\varepsilon_{\rm r} = 44.9 \pm 5\%$ and $\sigma = 0.85 \pm 5\%$) when the antenna has been designed to be matched to chip.1. Antenna sizes: $a = 15\ \mathrm{mm}$, $b = 20\ \mathrm{mm}$, $g = 3\ \mathrm{mm}$ Data refer to the full-size antenna (measurement data have been doubled). Markers at 850, 870, 910, 950 MHz.

VIII. Conclusions

The proposed antenna configuration seems to be attractive to achieve effective conjugate impedance matching to different kind of microchips without affecting the external size. Preliminary simulations have demonstrated that, provided the microchip transmitter is sensitive enough (RF activation power equal or less than 10 μW), the tag may be activated from a distance of 3 m up to 10 m depending on the mutual position between the reader and the tag. This could permit continuous monitoring of a moving human subject in a large room or within a medium-size corridor.

The activation distance is affected by the size of the human body due to power dissipation which causes a larger reduction of antenna gain for large bodies.

When the NSSP geometry is tuned to microchip transmitters with small and medium reactance, the resulting antenna exhibits a bandwidth large enough to cover the worldwide UHF RFID range, including Europe, the USA and Japan. These features have also been verified experimentally by measurements of a fabricated device radiating into a liquid phantom simulating human tissues.

The significant metallization area available in the NSSP geometry makes the proposed antenna a good candidate to host sensors and the required electronics.

ACKNOWLEDGMENT

The author wishes to thank J. Johnson for valuable discussions, G. Lovisolo, R. Pinto, and S. Mancini, of the Section of Toxicology and Biomedical Sciences of the ENEA Casaccia Research Centre, for their enthusiastic support in performing experimental measurements.

REFERENCES

[1] L. Cheng-Ju, L. Li, C. Shi-Zong, W. Chi Chen, H. Chun-Huang, and C. Xin-Mei, "Mobile healthcare service system using RFID," in *IEEE Int. Conf. Networking Sensing and Control* , 2004, vol. 2, pp. 1014–1019.

[2] R. S. Sangwan, R. G. Qiu, and D. Jessen, "Using RFID tags for tracking patients, charts and medical equipment within an integrated health delivery network," in *IEEE Int. Conf. Networking Sensing and Control*, 2004, pp. 1070–1074.

[3] P. E. Ross, "Managing care through the air," *IEEE Spectrum*, vol. 41, no. 12, pp. 26–31, Dec. 2004.

[4] K. Van Laerhoven, B. P. L. Lo, and J. W. P. Ng *et al.*, "Medical healthcare monitoring with wearable and implantable sensors," in *3rd Int. Workshop on Ubiquitous Computing for Pervasive Healthcare Applications (UbiHealth)* [Online]. Available: http://www.healthcare.pervasive.dk/ubicomp2004/papers/final_papers/laerhoven.pdf

[5] J. Park, J. Seol, and Y. Oh, "Design and implementation of an effective mobile healthcare system using mobile and RFID technology," in *Proc. 7th Int. Symp. HEALTCOM 2005*, pp. 263–266, 2205.

[6] S. Nambi, S. Nyalamadugu, S. M. Wentworth, and B. A. Chin, "Radio frequency identification sensors," in *Proc. 7th World Multiconf. Systemics, Cybernetics & Informatics (SCI 2003)*, 2003, pp. 386–390.

[7] C. Alippi and G. Vanini, "An application-level methodology to guide the design of intelligent-processing power-aware passive RFID," in *Proc. Int. Symp. on Circuits and Systems*, 2005, vol. 6, pp. 5509–5512.

[8] M. Philipose, J. Smith, B. Jiang, A. Mamishev, S. Roy, and K. Sundara- Rajan, "Battery-free wireless identification and sensing," *IEEE Pervasive Computing Mag.*, vol. 4, no. 1, pp. 10–18, 2005.

[9] J. W. P. Ng, B. P. L. Lo, O. Wells, M. Sloman, N. Peters, A. Darzi, C. Toumazou, and G. Yang, "Ubiquitous monitoring environment for wearable and implantable sensors (UbiMon)," in *Int. Conf. on Ubiquitous Computing (Ubicomp)*, 2004 [Online]. Available: www.ubicomp.org

[10] J. Kim and Y. Rahmat-Samii, "Implanted antennas inside a human body: Simulations, designs, and characterization," *IEEE Trans. Microw. Theory Tech.*, vol. 52, no. 8, pt. 2, pp. 1934–1943, Aug. 2004.

[11] Finkenzeller, RFID Handbook Wuket, 2000.

[12] G. Marrocco, "Gain-optimized self-resonant meander line antennas for RFID applications," *IEEE Antennas Wireless Propag. Lett.*, vol. 2, pp. 302–305, 2003.

[13] C. Cho, H. Choo, and I. Park, "Broadband RFID tag antenna with quasi-isotropic radiation pattern," *Electron. Lett.*, vol. 41, no. 20, pp. 1091–1092, Sep. 2005.

[14] H. W. Son and C. S. Pyo, "Design of RFID tag antennas using and inductively coupled feed," *Electron. Lett.*, vol. 41, no. 18, pp. 994–996, Sep. 2005.

[15] M. Hirvonen, P. Pursula, K. Jaakkola, and K. Laukkanen, "Planar inverted-F antenna for radio frequency identification," *Electron. Lett.*, vol. 40, no. 14, pp. 848–850, 2004.

[16] R. L. Li, G. DeJean, M. M. Tentzeris, and J. Laskar, "Integrable miniaturized folded antennas for RFID applications," in *Proc. IEEE Antennas Propag. Society Int. Symp.*, 2004, vol. 2, pp. 1431–1434.

[17] L. Ukkonen, D. Enels, L. Sydanheimo, and M. Kivikoski, "Planar wire-type inverted-F Rfid tag antenna mountable on metallic objects," in *Proc. IEEE Antennas Propag. Society Int. Symp.*, 2004, vol. 1, pp. 101–104.

[18] S. Jacobsen, P. R. Stauffer, and D. G. Newman, "Dual-mode antenna design for microwave heating and noninvasive thermometry of superficial tissue disease," *IEEE Trans. Biomed. Eng.*, vol. 47, no. 11, pp. 1500–1509, Nov. 2000.

[19] K. Maruyma, S. Mizushina, T. Sugiura, G. M. J Van Leeuwen, J. W. Hand, G. Marrocco, F. Bardati, A. D. Edwards, D. Azzopardi, and D. Land, "Feasibility of noninvasive measurement of deep brain temperature in newborn infants by multifrequency microwave radiometry," *IEEE Trans. Microw. Theory Tech.*, vol. 48, no. 11, pt. 1, pp. 2141–2147, Nov. 2000.

[20] S. C. Hagness, A. Taflove, and J. E. Bridges, "Three-dimensional FDTD analysis of a pulsed microwave confocal system for breast cancer detection: design of an antenna-array element," *IEEE Trans. Antennas Propag.*, vol. 47, no. 5, pp. 783–791, May 1999.

[21] K. Gosalia, G. Lazzi, and M. Humayun, "Investigation of microwave data telemetry link for a retinal prosthesis," *IIEEE Trans. Microw. Theory Tech.*, vol. 52, no. 8, pt. 2, pp. 1925–1933, Aug. 2004.

[22] P. V. Nikitin, K. V. S. Rao, S. F. Lam, V. Pillai, R. Martinez, and H. Heinrich, "Power reflection coefficient analysis for complex impedances in RFID tag design," *IEEE Trans. Microw. Theory Tech.*, vol. 53, no. 9, pp. 2715–2721, Sep. 2005.

[23] J. Curty, N. Joehl, C. Dehollain, and M. J. Delercq, "Remotely powered addressable UHF RFID integrated system," *IEEE J. Solid-State Circuits*, vol. 40, no. 11, pp. 2193–2202, Nov. 2005.

[24] C. Gabriel, S. Gabriel, and E. Corthout, "The dielectric properties of biological tissues: I. Literature survey," *Phys. Med. Biol.*, vol. 41, no. 11, pp. 2231–2249, Nov. 1996.

[25] B. G. Porter and S. S. Gearhart, "Impedance and polarization characteristics of H and IHI slot antennas," *IEEE Trans. Antennas Propag.*, vol. 48, no. 8, pp. 1272–1274, Aug. 2000.

[26] G. Marrocco and F. Bardati, "BEST: A finite-difference solver for time electromagnetics," *Simulation Practice Theory*, no. 7, pp. 279–293, 1999.

[27] S. Ramo, J. R. Whinnery, and T. Van Duzer, *Fields and Waves in Communication Electronics*, 3rd ed. New York: Wiley, 1994, pp. 474–475.

[28] L. Gil-Young Lee, K. Yonghoon, L. Jong-Sik, and N. Sangwook, "Size reduction of microstrip-fed slot antenna by inductive and capacitive loading," in *Proc. IEEE Antennas and Propagation Soc. Int. Symp.*, 2003, vol. 1, pp. 312–315.

[29] S. Basat, S. Bhattacharya, A. Rida, S. Johnston, L. Yang, M. M. Tentzeris, and J. Laskar, "Fabrication and assembly of a Novel high-efficiency UHF RFID tag on flexible LCP substrate," in *Proc. Electronic Components and Technology Conf.*, 2006, pp. 1352–1355.

[30] H. W. Son, J. Yeo, G. Y. Choi, and C. S. Pyo, "A low-cost, wideband antenna for passive RFID tags mountable on metallic surfaces," in *Proc. IEEE Antennas and Propagation Soc. Symp.*, 2006, pp. 1019–1022.

[31] Karthaus and M. Fischer, "Fully integrated passive UHF RFID transponder IC With 16.7- μW minimum RF input power," *IEEE J. Solid-State Circuits*, vol. 38, no. 10, pp. 1602–1608, Oct. 2003.

[32] M. Guelfi, F. Apollonio, N. Grazioli, S. Nocentini, G. Marrocco, and G. A. Lovisolo, "Dosimetric procedures for compliance tests of mobile communication devices," *Phys. Med.*, vol. XIII, no. 1, pp. 11–16, 1997.

[33] G. A. Lovisolo, R. Pinto, L. Ardoino, and S. Mancini, "Dosimetric techniques for the evaluation of the E.M. power absorption induced by cellular phones," *Radiat. Prot. Dosim.*, vol. 97, no. 4, pp. 369–374, 2001.

[34] G. Hartsgrove, A. Kraszewsky, and A. Surowiec, "Simulated biological materials for electromagnetic radiation absorption studies," *Bioelectromagnetics*, vol. 8, no. 4, pp. 29–36, 1987.

Gaetano Marrocco (M'98) received the Laurea degree in electronic engineering and the Ph.D. degree in applied electromagnetics from the University of L'Aquila, Italy, in 1994 and 1998, respectively.

Since 1997, he has been a Researcher at the University of Rome "Tor Vergata," Rome, where he currently teaches Antenna Design and Bioelectromagnetics. In summer 1994, he was at the University of Illinois at Urbana–Champain as a Postgraduate Student. In autumn 1999, he was a Visiting Researcher at the Imperial College in London, U.K. His research is mainly directed to the modelling and design of broad band and ultra wideband antennas and arrays as well as of miniaturized antennas for RFID applications. He has been involved in several space, avionic and naval programs of the European Space Agency, NATO, Italian Space Agency, and the Italian Navy. He holds two patents on broadband naval antennas.